

## EXPERIMENTS WITH SEVERAL ELEMENTS FOR VISCOUS INCOMPRESSIBLE FLOWS

M. FORTIN

*Departement de Math., Université Laval, Québec, G1K 7P4, Canada*

AND

A. FORTIN

*Departement de Math. Appliquées, Ecole Polytechnique, C. P. 6079 Succ. "A", Montréal, Canada H3C 3A7*

### SUMMARY

We present a numerical procedure to eliminate internal nodes from elements designed to approximate incompressible flow problems. We compare six elements in academic and industrial like flow problem and we discuss their relative qualities. A surprising conclusion is that richer elements may behave less well than simple ones if a good enforcement of incompressibility is not maintained.

KEY WORDS Incompressible Finite Elements

### INTRODUCTION

Finite element methods are now widely used for fluid flow problems. During the last fifteen years, many elements have been tested more or less successfully and it is certainly not possible to compare all of them. Experience has however shown that only a few of them led to efficient computations. For two-dimensional flows and quadrilateral elements for example, the  $Q_1-P_0$  (bilinear velocity, piecewise constant pressure) and the  $Q_2^{(9)}-P_1$  (biquadratic velocity, piecewise linear pressure) are now very popular even though the first one is known to develop spurious pressure modes<sup>1</sup> under some circumstances.

Mathematical analysis of elements used in fluid flow computations is centered on the inf-sup stability condition of Brezzi<sup>2</sup> and Babuška.<sup>3</sup> Recent papers<sup>4,5</sup> have pointed out that this condition can be obtained under quite general conditions by adding internal nodes to elements. In the case of discontinuous pressure, this enrichment procedure supposes that the element is already stable for the piecewise constant part of the pressure field. We shall make explicit in the present paper how these enriched elements can be implemented with only a few modifications of a standard code at almost no extra cost.

Knowing which elements are stable is not however, by far, a complete picture of the situation. Another important point is to get accurate results for high enough Reynolds numbers (which is not the same as getting numbers out of the computer).

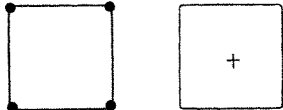
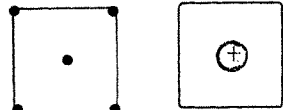
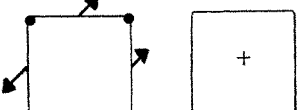
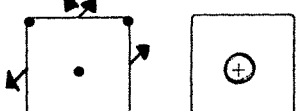
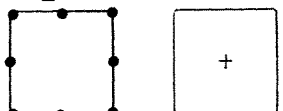
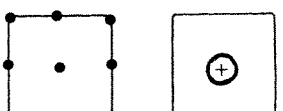
This paper presents numerical comparisons between elements that can be considered as members of a family containing at one end the  $Q_1-P_0$  element and at the other end, the  $Q_2^{(9)}-P_1$  element. Using the technique of the first part, they can all be reduced, for computational purposes, to their piecewise constant analogues. Some of these elements are stable and some are not. We

shall try to deduce from numerical experiments some guidelines to users that should also be useful when building elements for three-dimensional problems.

PRESENTATION OF THE ELEMENTS

Six different quadrilateral elements have been tested. Among them, three are already well known, namely the  $Q_1-P_0$ ,  $Q_2-P_0$  and  $Q_2^{(9)}-P_1$  elements. The last three are new elements. The  $R_2-P_0$  element is a non-standard element that has been introduced by Fortin.<sup>6</sup> The degrees of freedom are the velocities at the four vertices and the normal components of the velocity at the mid-side nodes. The last two, the  $R_2^+-P_1$  and  $Q_1^+-P_1$  are obtained from the  $Q_1-P_0$  and  $R_2-P_0$  elements, respectively, by adding an internal velocity node and by using piecewise linear pressure. The reader will find in Table I a complete description of all these elements. Finally, Figure 1 shows how these elements are interconnected, an arrow between two elements meaning that the last one is in some sense an enriched version of the first one.

Table I

Element	D.O.F.	Order of convergence	Constraint ratio on $n \times n$ mesh	B.B. condition
$Q_1-P_0$		$O(h)$	$\frac{1}{2}$	No
$Q_1^+-P_1$		$O(h)$	$\frac{3}{4}$	No
$R_2-P_0$		$O(h)$	$\frac{1}{4}$	Yes
$R_2^+-P_1$		$O(h)$	$\frac{1}{2}$	Yes
$Q_2-P_0$		$O(h)$	$\frac{1}{6}$	Yes
$Q_2^{(9)}-P_1$		$O(h^2)$	$\frac{3}{8}$	Yes

● Velocity node  
 ⤴ Normal velocity node

+ Constant pressure  
 ⊕ Linear pressure

\* This convergence result holds for regular or almost regular meshes.<sup>7</sup>

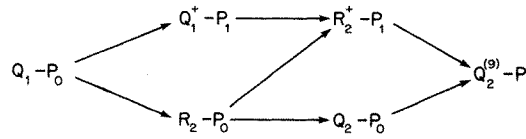


Figure 1

We give in Table I the so-called constraint ratio of the elements, that is the ratio of pressure d.o.f. to velocity d.o.f. on an  $n \times n$  mesh for large  $n$ . Although this is only indicative, a small ratio implies a poor enforcement of the divergence-free constraint.

This list is obviously not exhaustive. For instance we could consider elements such as the  $Q_2^+ - Q_1$  and the  $Q_2^+ - P_2$  introduced in Reference 5. These elements are also built by adding an appropriate number of internal nodes in order to satisfy the Babuška–Brezzi condition. It is also noteworthy that the same discussion could be applied to triangular elements. In that case, the  $P_2^+ - P_1$  element of Crouzeix and Raviart<sup>8</sup> plays essentially the same role as the  $Q_2^{(9)} - P_1$  for quadrilateral elements.

*Remark 1*

For linear pressure, we write for each element  $K$  (with centroid  $(\bar{x}, \bar{y})$ ).

$$P_K(x, y) = a_0 + a_1(x - \bar{x}) + a_2(y - \bar{y}), \tag{1}$$

which is different from the standard approximation on the reference element

$$\hat{P}(\hat{X}, \hat{Y}) = a_0 + a_1\hat{X} + a_2\hat{Y}, \tag{2}$$

along with

$$P_K(x, y) = \hat{P} \circ F_K^{-1}, \tag{3}$$

on each element. In (3),  $F_K$  is the transformation of co-ordinates mapping the reference element  $\hat{K}$  onto  $K$ . These two approximations yield the same order of convergence but (1) is more convenient for the elimination procedure described in the next section. ■

*Remark 2*

The  $Q_1^+ - P_1$  element is closely related to the 4-CST element discussed by Kikuchi<sup>9</sup> (see Figure 2)

This element is built by dividing a quadrilateral into four triangles. The degrees of freedom for the velocity are the same as those of the  $Q_1^+ - P_1$  element, and piecewise constant pressures are used on each triangle. However, a local checkerboard mode is present leaving only three independent degrees of freedom for pressure. A global checkerboard is also present on regular meshes, as in the  $Q_1 - P_0$  element. The analysis of Reference 7 could probably be extended to this element. ■

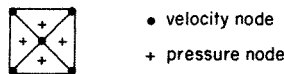


Figure 2

## ELIMINATION OF INTERNAL NODES BY A CHANGE OF SHAPE FUNCTION

In this section, we shall show that the addition of internal nodes has only a marginal effect on computational cost. We shall indeed show how a modification of shape functions enables the user to eliminate both the velocity internal nodes and the non-constant part of the pressure field. To understand the idea, it will be easier to go back to the Stokes problem:

$$\int_{\Omega} \mathbf{D}(\mathbf{u}) : \mathbf{D}(\mathbf{v}) dx - \int_{\Omega} p \nabla \cdot \mathbf{v} dx = \int_{\Omega} \mathbf{f} \cdot \mathbf{v} dx, \quad \forall \mathbf{v} \in V, \quad (4)$$

$$\int_{\Omega} q \nabla \cdot \mathbf{u} dx = 0, \quad \forall q \in L^2(\Omega), \quad \mathbf{u} \in V, \quad p \in L^2(\Omega). \quad (5)$$

The function space  $V$  is supposed to be chosen correctly with respect to the boundary conditions of the problem at hand. *Let us then consider the linear subspace  $V_0$  of divergence-free vector functions.* Problem (4), (5) can now be written in the equivalent form

$$\int_{\Omega} \mathbf{D}(\mathbf{u}) : \mathbf{D}(\mathbf{v}) dx = \int_{\Omega} \mathbf{f} \cdot \mathbf{v} dx, \quad \forall \mathbf{v} \in V_0. \quad (6)$$

From the numerical point of view, one could then eliminate pressure if an explicit construction of the discrete counterpart of  $V_0$  were known. This is however in general quite intricate to find and we refer the reader to References 10 and 11 for details. We shall follow that idea *only partially*.

Let us denote by  $M$  the subspace in  $L^2(\Omega)$  of piecewise constant functions and let  $N$  be its orthogonal complement. We can define

$$V_{0,N} = \left\{ \mathbf{v} \mid \mathbf{v} \in V, \int_{\Omega} q \nabla \cdot \mathbf{v} dx = 0, \quad \forall q \in N \right\}, \quad (7)$$

which is a subspace of  $V$ . It is then straightforward that (4), (5) can now be written as

$$\int_{\Omega} \mathbf{D}(\mathbf{u}) : \mathbf{D}(\mathbf{v}) dx - \int_{\Omega} \bar{p} \nabla \cdot \mathbf{v} dx = \int_{\Omega} \mathbf{f} \cdot \mathbf{v} dx, \quad \forall \mathbf{v} \in V_{0,N}, \quad \mathbf{u} \in V_{0,N}, \quad (8)$$

$$\int_{\Omega} \bar{q} \nabla \cdot \mathbf{u} dx = 0, \quad \forall \bar{q} \in M, \quad \bar{p} \in M. \quad (9)$$

We have thus reduced our problem to the case of a piecewise constant pressure field. As we shall see, building a basis for the discrete counterpart of  $V_{0,N}$  is a simple task that will not be performed explicitly. Moreover, once  $\mathbf{u}$  and  $\bar{p}$  are known, one can use, if needed, equation (4) to recover the non constant components of pressure.

*Remark 3*

This process is closely related to static condensation, but it differs in an important way: recovery of the  $N$  part of  $p$  can be avoided. Computations can be performed using analogues of (8), (9) without the need of knowing the value of the eliminated nodes. If needed, the non-constant components of pressure can be computed afterwards—element by element. ■

Let us now see how this idea can be implemented in the discrete case. If  $Q_h$  denotes the space of discrete pressures, we can write (for discontinuous pressure approximations)

$$Q_h = M + N_h, \quad (10)$$

where  $N_h$  is the non-constant part of the pressure. We can also define

$$V_{0,N_h} = \left\{ \mathbf{v}_h \mid \mathbf{v}_h \in \mathbf{V}_h, \int_{\Omega} q_h \nabla \cdot \mathbf{v}_h \, dx = 0, \forall q_h \in N_h \right\}. \tag{11}$$

For the sake of simplicity, we shall concentrate on the  $Q_1^+ - P_1$  element but the procedure described here is completely general and works as well for the  $R_2^+ - P_1$  and  $Q_2^{(9)} - P_1$  elements (see Remark 7). Let  $\mathcal{T}_h$  be a partition of the domain  $\Omega$  into quadrilaterals. For every  $K \in \mathcal{T}_h$ , we can write

$$\mathbf{u}_h(x, y)|_K = \sum_{i=1}^{10} \alpha_i \mathbf{N}_i(x, y), \tag{12}$$

where the  $\alpha_i$  and  $\mathbf{N}_i$  denote, respectively, the degrees of freedom and shape functions associated with  $K$ . (We shall assume that  $\mathbf{N}_9$  and  $\mathbf{N}_{10}$  are related to the internal node).

*Remark 4*

It is more usual to write

$$\mathbf{u}_h(x, y)|_K = \left( \sum_{i=1}^5 u_i \phi_i(x, y), \sum_{i=1}^5 v_i \phi_i(x, y) \right), \tag{13}$$

where  $\phi_i$  denotes the standard shape function associated with the  $i$ th node. Equation (12) is clearly equivalent if we set

$$\begin{aligned} \mathbf{N}_1 &= (\phi_1, 0), \quad \mathbf{N}_2 = (0, \phi_1), \quad \mathbf{N}_3 = (\phi_2, 0), \text{ etc.} \\ \alpha_1 &= u_1, \quad \alpha_2 = v_1, \quad \alpha_3 = u_2, \text{ etc.} \end{aligned} \tag{14}$$

As we shall see, our elimination procedure will be equivalent to modify both components of the  $\mathbf{N}_i$  and thus (12) is more suitable for our purpose. ■

In this particular case of the  $Q_1^+ - P_1$  element, we have linear discontinuous pressure. Consequently, the discrete divergence-free condition can be written (see Remark 1), for arbitrary coefficients  $a_{0K}$ ,  $a_{1K}$  and  $a_{2K}$

$$\sum_{i=1}^{10} \alpha_i \int_K (a_{0K} + a_{1K}(x - \bar{x}) + a_{2K}(y - \bar{y})) \nabla \cdot \mathbf{N}_i \, dx = 0, \quad \forall K \in \mathcal{T}_h. \tag{15}$$

The above equation will in turn be satisfied if

$$\sum_{i=1}^{10} \alpha_i \int_K \nabla \cdot \mathbf{N}_i \, dx = 0, \quad \forall K \in \mathcal{T}_h, \tag{16}$$

$$\sum_{i=1}^{10} \alpha_i \int_K (x - \bar{x}) \nabla \cdot \mathbf{N}_i \, dx = 0, \quad \forall K \in \mathcal{T}_h, \tag{17}$$

$$\sum_{i=1}^{10} \alpha_i \int_K (y - \bar{y}) \nabla \cdot \mathbf{N}_i \, dx = 0, \quad \forall K \in \mathcal{T}_h. \tag{18}$$

Condition (16) corresponds to the discrete divergence-free condition for piecewise constant pressure. Moreover, (17) and (18) are the necessary and sufficient conditions for  $\mathbf{V}_h$  to belong to  $V_{0,N_h}$ . The idea is now to determine  $\alpha_9$  and  $\alpha_{10}$  in order that these last two equations are

automatically satisfied. Indeed, setting

$$X_i = \int_K (x - \bar{x}) \nabla \cdot \mathbf{N}_i \, dx, \quad (19)$$

$$Y_i = \int_K (y - \bar{y}) \nabla \cdot \mathbf{N}_i \, dx, \quad (20)$$

and integrating by parts, we easily obtain

$$0 = X_{10} = Y_9, \quad X_9 = Y_{10}, \quad \forall K \in \mathcal{T}_h. \quad (21)$$

Equations (17) and (18) may thus be rewritten as

$$\alpha_9 = \frac{-1}{X_9} \sum_{i=1}^8 \alpha_i X_i, \quad \alpha_{10} = \frac{-1}{X_9} \sum_{i=1}^8 \alpha_i Y_i. \quad (22)$$

We finally conclude, using (12) and (22) that

$$\mathbf{v}_h|_K = \sum_{i=1}^8 \alpha_i \left( \mathbf{N}_i - \frac{X_i}{X_9} \mathbf{N}_9 - \frac{Y_i}{X_9} \mathbf{N}_{10} \right) = \sum_{i=1}^8 \alpha_i \mathbf{N}'_i. \quad (23)$$

In the above equation, the sum is over 8 nodes (the internal one is eliminated). From our construction, the  $\{\mathbf{N}'_i\}_{i=1}^8$  constitute a basis for  $V_{0,N_h}$  and it is thus possible to use the formulation (8), (9) to solve our problem. It must be pointed out that as  $\mathbf{N}_9$  and  $\mathbf{N}_{10}$  vanish on the boundary, the coefficients  $\alpha_i$  remain velocity components at nodes 1 to 8.

*Remark 5*

Unlike the standard basis functions  $\mathbf{N}_i$ , the  $\mathbf{N}'_i$  have two non-zero components (they are ‘true’ vectors). At first sight, this may lead to heavy computations but as well shall see, it is not necessary to use them directly. ■

*Remark 6*

This method is particularly well adapted to the penalty technique since we are left with piecewise constant pressure. Moreover, the penalty factor remains exactly the same as for the  $Q_1-P_0$  element, since the shape functions  $\mathbf{N}_9$  and  $\mathbf{N}_{10}$  are *already divergence-free on average*. ■

Let us now show how it is possible to use our elimination method without explicitly building the shape functions  $\mathbf{N}'_i$ . Indeed, the  $\mathbf{N}'_i$  are merely linear combinations of the initial shape functions  $\mathbf{N}_i$ . Consequently, let  $\mathbf{A}_{10 \times 10}$  be the standard elementary matrix (using one-component shape functions) associated with the  $Q_1^+ - P_1$  element. Each element  $a_{ij}$  of  $\mathbf{A}$  is of the form

$$a_{ij} = \mathbf{a}(\mathbf{N}_i, \mathbf{N}_j), \quad (24)$$

where  $\mathbf{a}$  is the bilinear form associated with the variational formulation. Using the shape functions  $\mathbf{N}'_i$  is thus equivalent to constructing a new matrix  $\mathbf{a}'$  such that

$$a'_{ij} = \mathbf{a}(\mathbf{N}'_i, \mathbf{N}'_j) = a_{i,j} - \frac{X_i}{x_a} a_{i,9} - \frac{Y_i}{X_9} a_{i,10} - \frac{X_j}{X_9} a_{9,j} - \frac{Y_j}{Y_9} a_{10,j}. \quad (25)$$

This can be done by post-processing, at element level, the rows and the columns of the matrix  $\mathbf{A}$ . For instance, the 9th and 10th columns of  $\mathbf{A}$  are multiplied by  $X_i/X_9$  and  $Y_i/X_9$ ,

respectively and the result is subtracted from the  $i$ th column. The same operation is done on the rows (it is not important to process either the rows or columns first). Once the post-processing is done, the last two rows and columns can be discarded.

We conclude from all this that only a few modifications are needed to implement our method in a standard  $Q_1-P_0$  code. One merely has to add a new shape function at the centroid of the reference element and to post-process on the rows and columns of the elementary matrix (the coefficients  $X_i$  and  $Y_i$  can be computed once and for all in a pre-processing code).

Since our method works as well for the  $Q_2^{(9)}-P_1$  and  $R_2^+-P_1$  elements, from a computational standpoint we have reduced, respectively, (up to the cost of pre-processing) the  $Q_2^{(9)}-P_1$  element to the  $Q_2^{(8)}-P_0$  element, the  $R_2^+-P_1$  element to the  $R_2-P_0$  element, and the  $Q_0^+-P_1$  element to the  $Q_1-P_0$  element. As we shall see in the next section, this small extra computational cost may lead to a substantial gain in accuracy.

*Remark 7*

As already pointed out, this method can also be used when we have more than one internal node (the  $Q_2-P_2$  element for instance). In such a case, the elimination of the internal nodes requires the solution of a small linear system on each element. Moreover, it is then necessary to use the analogue of equation (1), otherwise, the linear system may be singular. ■

NUMERICAL RESULTS

To illustrate our purpose, we have considered three numerical tests, each one having its particular difficulties. Our first problem is the Poiseuille flow, which is classical but gives rise to interesting conclusions; the next one, the no-flow test, was first considered by Gresho *et al.*<sup>12</sup> This is also a very simple problem and here again some elements yield surprising results. Finally, we have considered a more realistic (industrial) problem, the cascade flow.

*The Poiseuille flow*

Let us briefly describe the problem. A parabolic velocity profile is imposed at both the inlet and outlet of a rectangular channel. If  $H$  is the height of the canal, then the analytic solution of the Navier–Stokes equations is

$$\mathbf{u} = \left( \frac{4y}{H^2}(H - y), 0 \right), \quad p = \frac{-4x}{H^2} + \text{constant}. \tag{26}$$

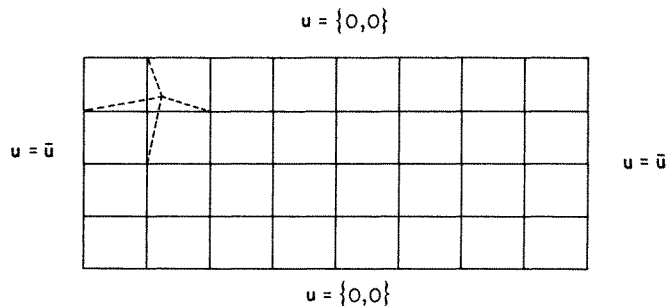


Figure 3

We present in Figure 3 the two meshes that have been used for the finite element discretization. The first one is a regular  $4 \times 8$  mesh and the other has been obtained by slightly displacing one point.

In our first attempt, we have used the  $Q_1-P_0$  element on the regular mesh. As one can see in Figure 4, the results are very good for both velocity and pressure fields.

However, on the distorted mesh, the pressure field is completely useless in that form, even though the velocity field is satisfactory (see Figure 4(c)). This is a visualization of an impure spurious pressure mode in the sense of Sani *et al.*<sup>1</sup>

We have next used the  $R_2-P_0$  element (which satisfies the B.B. condition) and the results are presented in Figure 4(e) for the pressure on the second mesh (the velocity field is very similar to the one for the  $Q_1-P_0$  element). We have also tested this element on a very distorted mesh and the results were still very good.

It should be noticed that spurious pressure can be filtered but accuracy is strongly affected (Figure 4(f)). We refer the reader to the works of Stenberg and Pitkaranta<sup>7</sup> for convergence analysis of such pathological cases. This shows that choosing an element with stable pressure

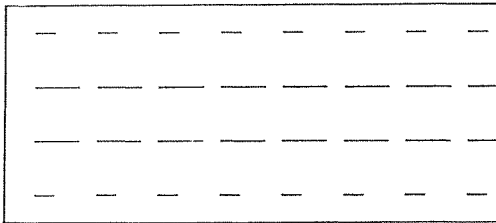


Figure 4(a). Velocity field, regular mesh ( $Q_1-P_0$ ) element

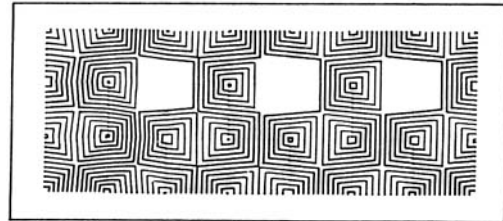


Figure 4(d). Pressure field, distorted mesh ( $Q_1-P_0$ ) element

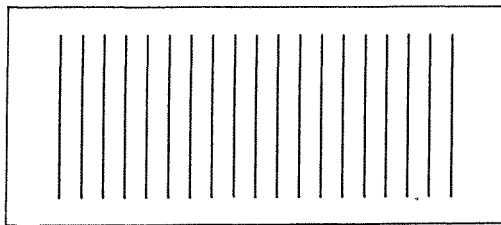


Figure 4(b). Pressure field, regular mesh ( $Q_1-P_0$ ) element

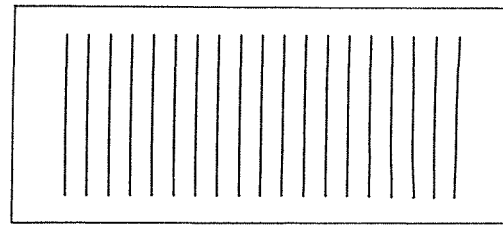


Figure 4(e). Pressure field, distorted mesh ( $R_2-P_0$ ) element

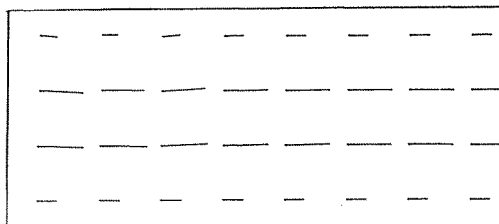


Figure 4(c). Velocity field, distorted mesh ( $Q_1-P_0$ ) element

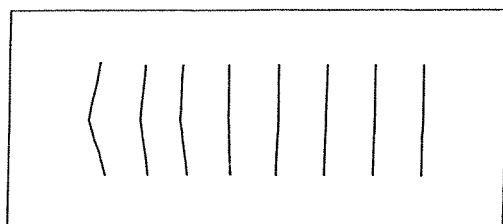


Figure 4(f). Filtered pressure field, distorted mesh ( $Q_1-P_0$ ) element



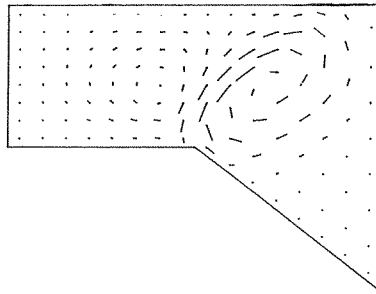


Figure 5

is an advantage but is not absolutely necessary and that the  $Q_1-P_0$  element can be used if it enjoys some other qualities.

#### *The no-flow test<sup>12</sup>*

On the boundary  $\Gamma$  of the domain  $\Omega$  of Figure 5, we impose homogeneous boundary conditions  $\mathbf{u} = \mathbf{0}$  and we let  $\mathbf{f} = (0, g)$  (non-zero external forces). Here again, the analytic solution of the Navier–Stokes equations is known, that is

$$\mathbf{u} = \mathbf{0}, \quad p = gy + c. \quad (27)$$

Using an  $8 \times 16$  mesh with the  $Q_1-P_0$  and  $R_2-P_0$  elements, we get  $O(h)$  vortices illustrated in Figure 5. The problem here is not due to a failure in satisfying the B.B. condition but to the fact that we are using only piecewise constant pressure. Consequently, the linear analytic pressure cannot be reproduced exactly and we have a striking example of the dependency of the approximation of the pressure. It is clear that the cure to this is to use piecewise linear (at least) pressure. Indeed, the  $Q_1^+-P_1$  element passes the no-flow test remarkably well, yielding the exact solution for both velocity and pressure (without checkerboarding!).

#### *Remark 8*

One could hastily conclude from the above discussion that the  $Q_1^+-P_1$  element should give the exact solution for the Poiseuille flow on a distorted mesh. Unfortunately, this is not the case since the velocity space  $V_h$  does not contain the exact solution. Consequently, the  $Q_1^+-P_1$  element gives almost the same results as the  $Q_1-P_0$  element and the pressure remains step-wise constant (or almost). ■

#### *The cascade flow*

Our final test consists in simulating the flow between the blades of a turbomachine. For this problem, the velocity field is very important but the pressure field is fundamental since we are mostly interested in computing the head losses. Figure 6 displays the geometry and boundary conditions. The domain is in fact periodic and represents an infinite stack of similar domains. In the finite element code, periodicity is ensured by assigning the *same number* to degrees of freedom that are to be identified. They are thus taken as *identical* by the assembly routine.

In the tests performed we compare the results of various elements at different Reynolds numbers. It is soon apparent to anyone making such tests that variations of the parameter  $Re$

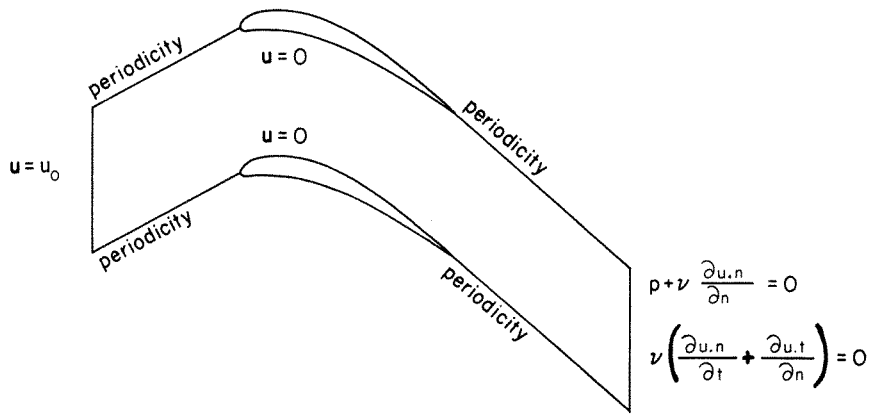


Figure 6

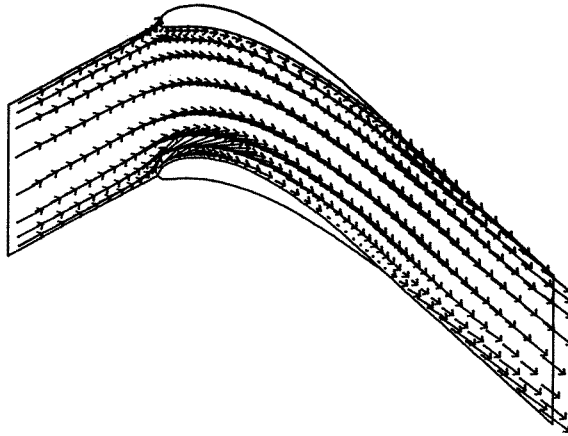


Figure 7(a).  $Q_1-P_0$  element,  $Re = 1000$

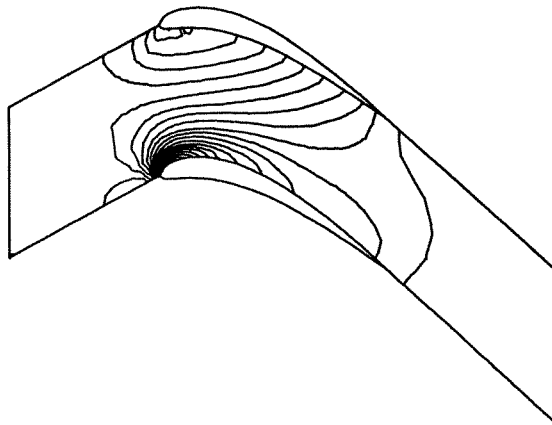


Figure 7(b).  $Q_1-P_0$  element,  $Re = 1000$

have very different effects depending on the element used. We summarize this by a concept of numerical diffusion defined by a purely phenomenological point of view: we say that an element  $E_1$  is more diffusive than  $E_2$  if the results of  $E_1$  at a Reynolds number  $Re_1$  are qualitatively similar to those of  $E_2$  at a lower Reynolds number  $Re_2$ . This diffusion can be traced to two sources, namely discretization of non-linear terms and discretization of the compressibility condition. We did not try to separate those closely intermixed causes.

We have tested the six previously described elements on an  $8 \times 49$  mesh. In the absence of experimental results, our criterion for comparison will be the  $Q_2^{(9)}-P_1$  element on a finer mesh ( $12 \times 64$ ), since this element has been shown to perform very well on various fluid flow problems. Figures 7–12 display the results at  $Re = 1000$  for all these elements except the  $R_2-P_0$  for which we could not reach Reynolds numbers higher than 400 (we lost convergence of our quasi Newton–Raphson algorithm). Finally, Figure 13 gives the results for the  $Q_2^{(9)}-P_1$  element on the finer mesh. Let us now analyse those results in detail. First, the  $Q_1-P_0$  and  $Q_1^+-P_1$  elements give very similar results. A too large stagnation region is observed on the leading edge of the blade and no vortices appear on the trailing edge. On a distorted mesh it is known<sup>6</sup> that the smallest computable vortex

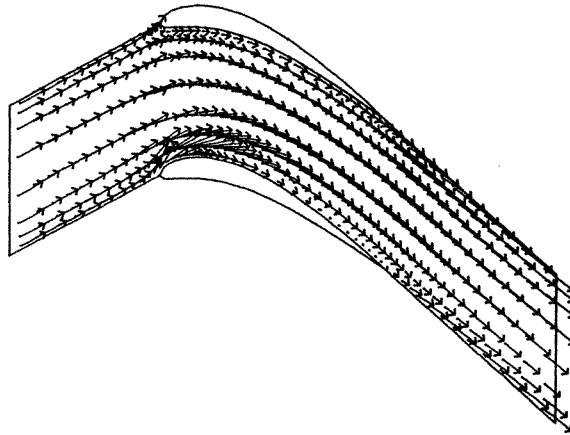


Figure 8(a).  $Q_1^+-P_1$  element,  $Re = 1000$

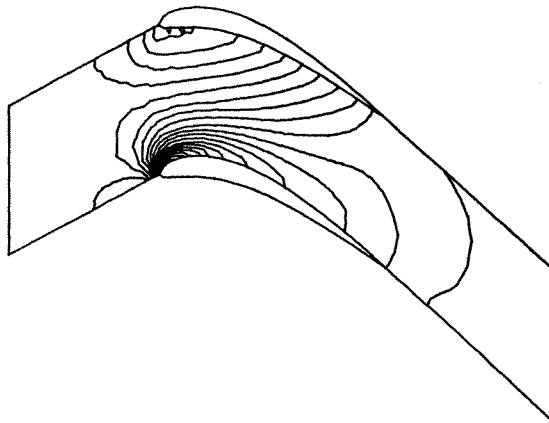
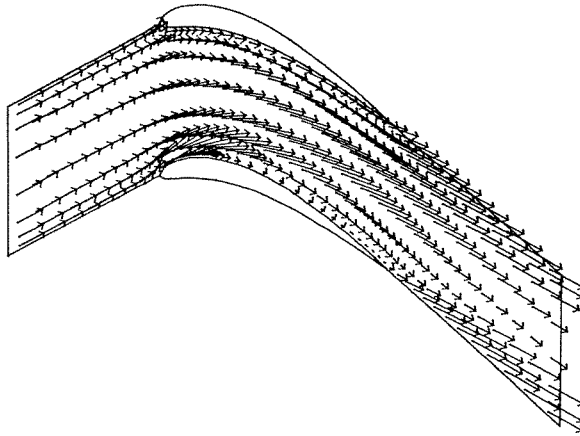
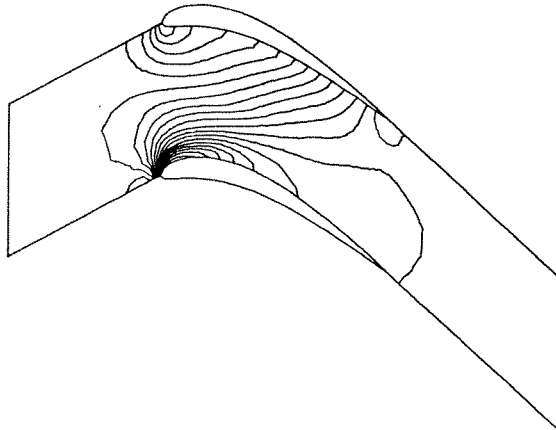
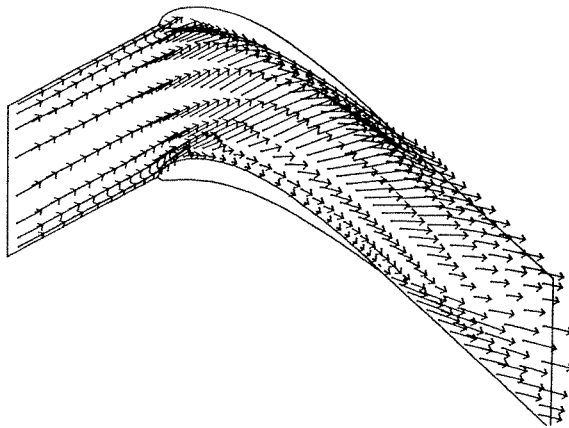


Figure 8(b).  $Q_1^+-P_1$  element,  $Re = 1000$

Figure 9(a).  $R_2-P_0$  element,  $Re = 400$ Figure 9(b).  $R_2-P_0$  element,  $Re = 400$ Figure 10(a).  $Q_2-P_0$  element,  $Re = 1000$

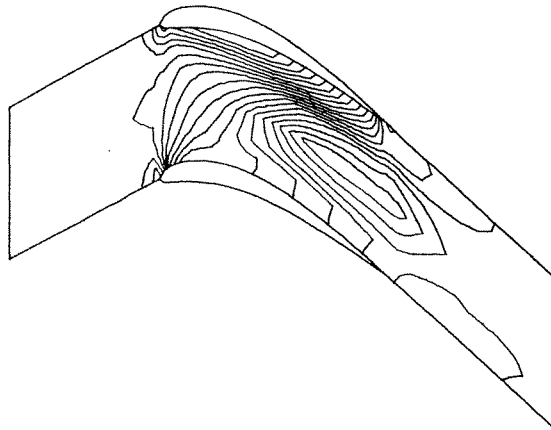


Figure 10(b).  $Q_2-P_0$  element,  $Re = 1000$

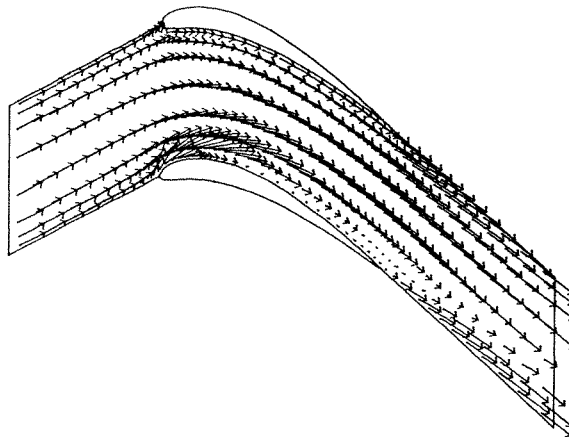


Figure 11(a).  $R_2^+-P_1$  element  $Re = 1000$

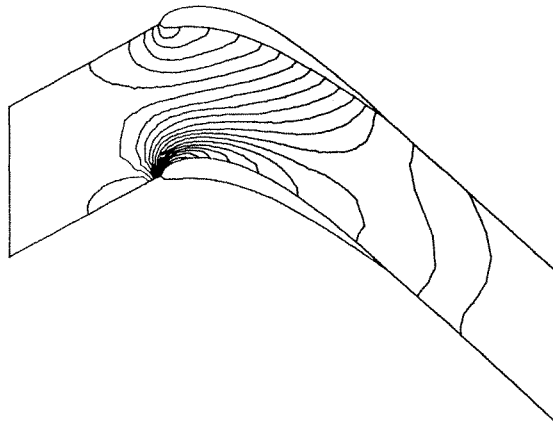
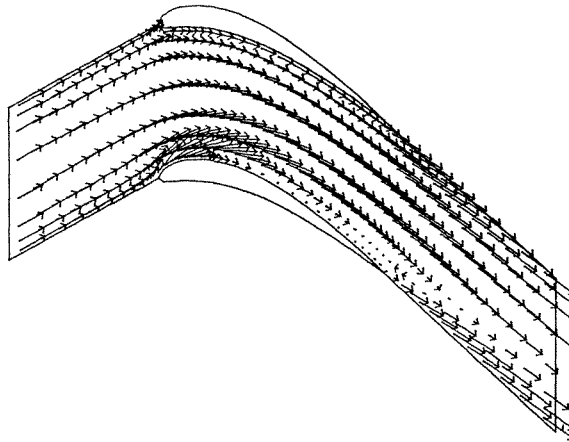
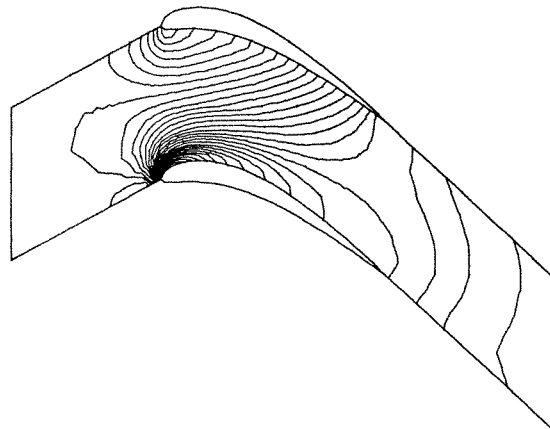
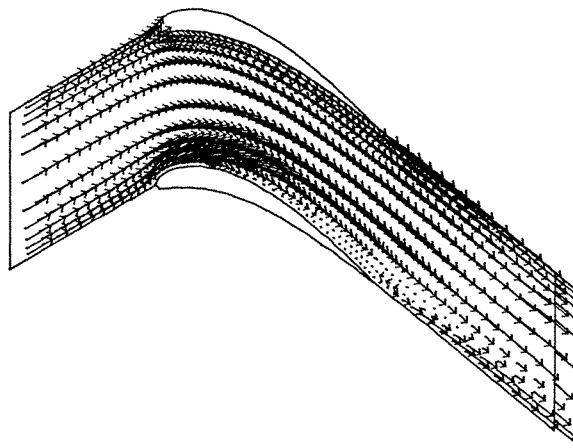


Figure 11(b).  $R_2^+-P_1$ ,  $Re = 1000$

Figure 12(a).  $Q_2^{(9)}$ - $P_1$  element,  $Re = 1000$ Figure 12(b).  $Q_2^{(9)}$ - $P_1$  element,  $Re = 1000$ Figure 13(a).  $Q_2^{(9)}$ - $P_1$  element,  $Re = 1000$  ( $12 \times 64$  mesh)

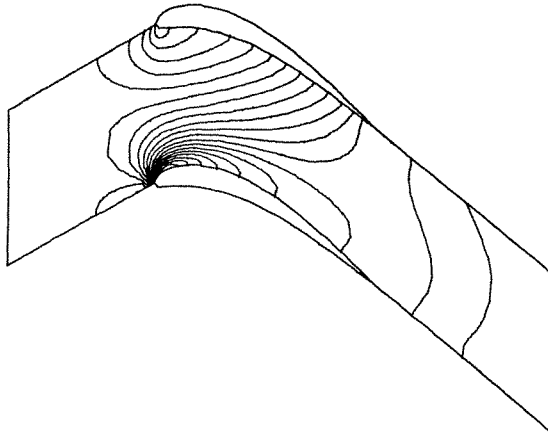


Figure 13(b).  $Q_2^0-P_1$  element,  $Re = 1000$  ( $12 \times 64$  mesh)

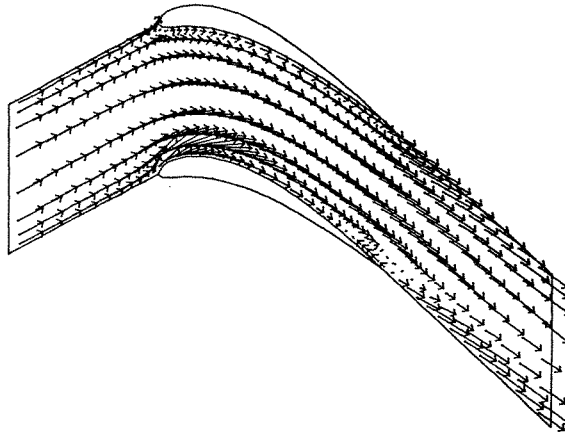


Figure 14.  $Q_1-P_0$  element,  $Re = 1800$

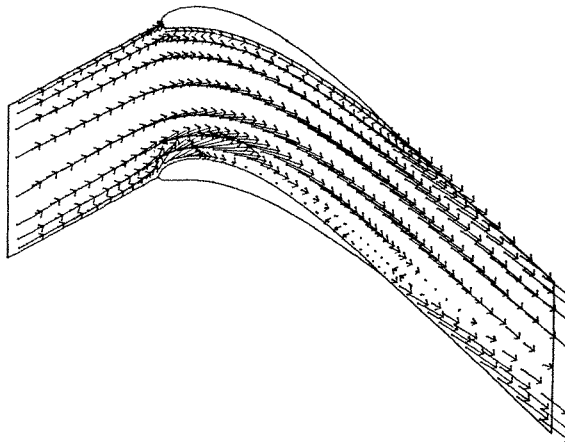


Figure 15.  $R_2^+-P_1$  element,  $Re = 1100$

needs a four by four patch of elements. This relative rigidity probably accounts for the stagnation region. For these elements, vortices appear only at Reynolds numbers higher than 1500 (see Figure 14); this means numerical diffusion in the above defined sense. As already pointed out, the pressure fields are acceptable after filtering even if some ripples remain.

The behaviour of the  $Q_2-P_0$  element is also very interesting. Here again, no vortices are developed, even at very high Reynolds numbers. Moreover, the flow between the blades is very different from the results obtained by other elements. The pressure field is, in turn, far from being similar to the 'real' pressure field of Figure 13. The reason for this surprising behaviour is that the discrete incompressibility condition

$$(q_h, \nabla \cdot \mathbf{u}_h) = 0, \quad \forall q_h \in Q_h, \quad (28)$$

is too weak, or, in other words, this element is too compressible. The solution is thus to enforce this incompressibility condition. We have seen in the previous section that this can be done by adding an internal velocity node and by using linear pressure. We obtain in that way the well-known  $Q_2^{(9)}-P_1$  element and it should be noticed that for this particular case, we start from a linear converging element to achieve a quadratic converging one. The results illustrated in Figure 12 are of course very close to those of Figure 13.

Let us now say a few words about the  $R_2-P_0$  and  $R_2^+-P_1$  elements. First, the  $R_2-P_0$  element is very disappointing since we cannot reach high Reynolds numbers. Furthermore, some experiments have shown that it suffers also from a too weak incompressibility condition. In contrast, the  $R_2^+-P_1$  element, which is numerically equivalent to the preceding one, is a remarkably good element. It also adds numerical diffusion but much less than the  $Q_1-P_0$  and  $Q_1^+-P_1$  elements. This is illustrated in Figure 15 where the results at  $Re = 1100$  are very similar to those of the  $Q_2^{(9)}-P_1$  element at  $Re = 1000$  (Figure 12).

#### Remark 9

The practical implementation of the  $R_2^+-P_1$  element is straightforward. One merely has to compute on each element the elementary matrix associated with the  $Q_2^{(9)}-P_1$  element and to post-process the rows and columns to eliminate the internal node (see the preceding section) and the tangential component of the velocity.

## CONCLUSION

For a given Reynolds number, we observe large differences in the flow computed using different elements. In particular, numerical diffusion is more or less important depending on the element. Another important point is the way the discrete incompressibility condition is imposed. A too weak condition may lead to very poor results. The reader must be aware that obtaining results at high Reynolds number is not in itself a good criterion for determining if an element is good or not. For instance, the  $Q_1-P_0$  and  $Q_1^+-P_1$  elements give results at very high Reynolds number but as we have seen, the accuracy is not satisfactory when compared to the  $Q_2^{(9)}-P_1$  element. Another important point is that enriching an element is not always valuable. For example, if we add four degrees of freedom to the  $Q_1-P_0$  element, which is an acceptable element, we obtain the  $Q_2-P_0$  element, which is too soft and much too diffusive.

Appreciating the  $Q_1-P_0$  element seems to be, at least partially, a matter of point of view. Taking as granted that spurious pressure modes can be filtered out, our experiments show that this element yields results quite comparable to those of other elements. It must however be remarked that this element is quite diffusive (in the above defined sense) and that to obtain the



same accuracy near the stagnation point a much finer mesh should be used. The advantage of this element is its low-cost implementation and may be also the possibility of using a low-order Gauss integration scheme in computing the elementary matrices.<sup>13</sup>

Adding an internal node and changing to linear pressure leads to the  $Q_1^+ - P_1$  element. The extra cost is low but the gain is also small. We however believe that the  $Q_1^+ - P_1$  should replace the  $Q_1 - P_0$ , for it is less sensitive to mesh distortion.

The  $R_2 - P_0$  and  $Q_2 - P_0$  element are very poor elements. If we compare to the  $Q_1 - P_0$ , the pressure has been stabilized but they are very sensitive to the mesh, particularly the  $R_2 - P_0$ . Moreover, the discrete *divergence free condition associated with these elements is also too weak* and consequently, the results obtained are in some cases completely wrong. These are other examples of the fact that enriching an element does not always lead to an improvement of quality.

Enriching the  $Q_2 - P_0$  element yields the  $Q_2^{(9)} - P_1$  element. In that particular case, we gain an order of convergence and it is already known that we have here a very good element (probably the best one for two-dimensional problems). Its major drawback could be its computational cost but it is not so clear since a coarser mesh is sufficient to get good result.

Finally, passing from the  $R_2 - P_0$  to the  $R_2^+ - P_1$  gives a remarkable improvement. We do not gain an order of convergence but we get results very similar to those of the  $Q_2^{(9)} - P_1$  element. This new element has, after elimination, only 12 degrees of freedom on each element and requires only a few modifications to a  $Q_2^{(9)} - P_1$  code. We thus believe that it is competitive from a cost-effectiveness standpoint.

The major conclusion of this work is that adding an internal node is always worth the cost if one uses the elimination method described here. Interestingly, a similar discussion is true for three-dimensional problems. Fortin<sup>6</sup> suggested the  $R_2 - P_0$  (3-D) element, which is a straightforward generalization of the  $R_2 - P_0$  (2-D). From our experience, we now believe that adding internal node(s) would give a much better element. This element could possibly compete with the  $Q_1 - P_0$  (3-D) element since it can be used at a still reasonable cost. It should also be noticed that the  $Q_2^{(27)} - P_1$  element has been shown to be too compressible. Extrapolating from our results for the  $Q_2 - P_0$  element we may believe that this softness probably leads to a large diffusiveness and that it will be necessary to use  $Q_1$  pressure to get accurate results with a second order three-dimensional element.

#### ACKNOWLEDGEMENT

This work was partly supported by NSERC (Canada) and by FCAC, (Québec)

#### REFERENCES

1. R. L. Sani, R. M. Gresho, R. L. Lee and D. F. Griffiths, 'The cause and cure (?) of the spurious pressures generated by certain FEM solutions of the incompressible Navier-Stokes equations: Part 1. *Int. j. numer. methods fluids*, **1**, 17-43 (1981).
2. F. Brezzi, 'On the existence, uniqueness and approximation of saddle point problems arising from Lagrangian multipliers', *RAIRO, Anal. Num.*, **8**, (R3).
3. I. Babuška, 'Error bounds for finite element method', *Numer. Math.*, 322-333 (1971).
4. F. Brezzi and G. Pitkaranta, 'On the stabilization of finite element approximations of the Stokes problem', in W. Hackbusch (ed.), *Efficient Solutions of Elliptic Systems*, Frieds. Viewey 1984, pp. 11-19.
5. M. Fortin, and A. Fortin, 'Newer and newer elements for incompressible flows', in J. T. Oden (ed.), *Finite Elements in Fluids*, Vol 6, Wiley, 1984.
6. M. Fortin, 'Old and new finite elements for incompressible flow', *Int. j. numer. methods fluids*, **1**, 347-364 (1981).
7. G. Pitkaranta and R. Stenberg, 'Error bounds for the approximation of the Stokes problem using bilinear-constant elements on irregular quadrilateral meshes', *University of Helsinki, Report MAT-A 222*, 1984.
8. M. Crouzeix and P. A. Raviart, 'Conforming and non-conforming finite element methods for solving the stationary Stokes equations', *RIARO, Anal. Num.*, **7**, (R3), 33-76 (1973).

9. N. Kikuchi, 'Remarks on 4CST-elements for incompressible materials', *Computer Meth. in App. Mech and Eng.*, **37**, 109–123 (1983).
10. D. F. Griffiths, 'The construction of approximately divergence-free finite elements', in A. Aziz (ed.) *The Mathematical foundations of the finite element method with applications to PDE*, Academic Press, 1972.
11. F. Hecht, 'Construction d'une base d'un élément fini  $P_1$  nonconforme à divergence nulle dans  $\mathbb{R}^3$ ', *Thèse de 3ième cycle*, Université Pierre et Marie Curie (Paris VI), 1980.
12. P. M. Gresho, R. L. Lee and R. L. Sani, 'Further studies in equal order interpolation for Navier–Stokes', *Fifth Int. Symposium on Finite Elements in Flow Problems*, Austin, Texas, 1984.
13. P. M. Gresho, S. T. Chan, R. L. Lee and C. D. Upson, 'A modified finite element method for solving the time-dependent incompressible Navier–Stokes equations. Part 1', *Int. j. numer. methods, fluids*, **4**, 557–598 (1984).